Inorganic Chemistry

ARTICLE

pubs.acs.org/IC

A New Organic−Inorganic Hybrid Oxyfluorotitanate [H*gua*]$_2$·($Ti_5O_5F_{12}$) as a Transparent UV Filter

J. Lhoste,[†,‡] X. Rocquefelte,[†] K. Adil,[‡] R. Dessapt,[†] S. Jobic,[†] M. Leblanc,[‡] V. Maisonneuve,*[,‡] and M. Bujoli-Doeuff*[,†]

[†]IMN, UMR 6502, 2 rue de la Houssinière, BP 32229, 44322 Nantes Cedex 3, France

[‡]LdOF, UMR 6010, Faculté des Sciences et Techniques, Université du Maine, Avenue O. Messiaen, 72085 Le Mans Cedex 09, France

Supporting Information

ABSTRACT: A new generation UV absorber is obtained by microwave-heating-assisted hydrothermal synthesis: [H*gua*]$_2$·($Ti_5O_5F_{12}$). The structure of this hybrid titanium(IV) oxyfluoride is ab initio determined from powder X-ray data by combining a direct space method, Rietveld refinement [orthorhombic, *Cmm*2, a = 22.410(1) Å, b = 11.191(1) Å, c = 3.802(1) Å], and density functional theory geometry optimization. The three-dimensional network is built up from infinite inorganic layers $_\infty$($Ti_5O_5F_{12}$) separated by guanidinium cations. The theoretical optical gap (3.2 eV) estimated from density of state calculations is in good agreement with the experimental gap (3.3 eV) obtained by UV−vis diffuse reflectivity. The optical absorption is mainly due to O(2p) → Ti(3d) and F(2p) → Ti(3d) transitions at higher energies. The refraction index is low in the visible range ($n \approx 1.9$) compared to that of TiO_2 and, consequently, [H*gua*]$_2$·($Ti_5O_5F_{12}$) shows a good transparency adapted to UV shielding. Under UV irradiation at 254 nm for 40 h, the white microcrystalline powder turns to light purple-gray. This color change is caused by the reduction of Ti^{IV} to Ti^{III}, confirmed by magnetic measurements.

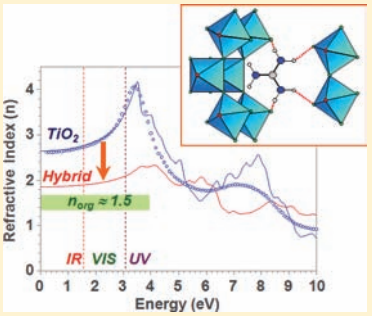

INTRODUCTION

During the last 10 years, a growing number of studies have been devoted to the development of new inorganic UV-absorber materials exhibiting simultaneously high absorption in the UV range and good transparency in the visible range. Such materials are of strong interest for industrials producing organic-based products (plastic, wood, etc.), which must be protected against UV-radiation deterioration for both indoor and outdoor applications.

Today, the UV-absorber material that is mainly used by industries is TiO_2. While this compound exhibits an adequate band gap for UV protection, it also shows a very high refractive index, i.e., n(rutile) = 2.7 and n(anatase) = 2.55. When such inorganic particles are incorporated into an organic medium, which exhibits a significantly smaller refractive index ($n \approx 1.5$), a whitening is observed, leading to a color degradation of the protected surface. To overcome such a problem, three strategies have been envisioned allowing one to increase the transparency in the visible-light region: (i) the reduction of the size of the particles up to the nanosize range (20−80 nm),[1−5] (ii) the development of new inorganic materials in which O^{2-} ions are substituted by ions exhibiting lower electron polarizabilities, such as F^- ions,[6,7] and (iii) the development of new hybrid organic−inorganic materials.[8] In our previous papers, seven TiO_2 varieties[9] and the fluorine-substituted phases $TiOF_2$ and TiF_4[6] have been considered by a dual approach combining energy loss spectroscopy (EELS) and density functional theory (DFT) electronic band structure calculations. These investigations have confirmed that it is possible to reduce the refractive index of the particles to values close to that of the organic medium, i.e., $n \approx 1.5−1.7$, by replacing high-scattering elements in the visible range with low-scattering ones and/or by increasing the volume of the unit cell and introducing large pores.

The present paper goes one step beyond, by proposing a system in which oxygen atoms are partially substituted by fluorine atoms and in which the inorganic blocks are separated by organic moieties, i.e., guanidinium cations. Herein, we report on the synthesis of a novel bidimensional inorganic−organic hybrid compound obtained with guanidine (*gua*, [H*gua*]$_2$·($Ti_5O_5F_{12}$). The crystal structure determination is based on an approach combining a direct space method, Rietveld refinement, and DFT-based geometry optimization. The electronic band structure is calculated and discussed in order to understand the origin of the optical properties. The optical gap is estimated using both UV−vis diffuse reflectivity and DFT calculations. Finally, the ability of [H*gua*]$_2$·($Ti_5O_5F_{12}$) to generate electron−hole pairs under UV irradiation at 254 nm is evaluated, and the resulting amount of Ti^{3+} ions is quantified using magnetic measurements.

EXPERIMENTAL SECTION

Materials. TiF_4 and guanidine hydrochloride $[C(NH_2)_3]Cl$ were obtained from Aldrich and used without further purification.

Synthesis. [H*gua*]$_2$·($Ti_5O_5F_{12}$) was synthesized from TiF_4, guanidine hydrochloride $[C(NH_2)_3]$·Cl (denoted as [H*gua*]·Cl), and

Received: February 28, 2011
Published: May 05, 2011

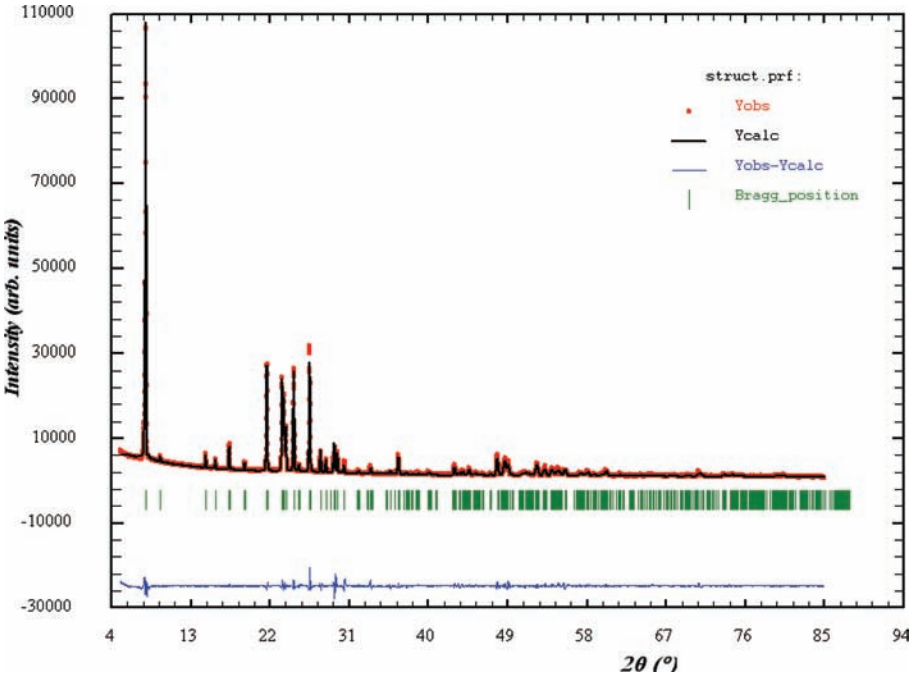

Figure 1. Final Rietveld profile refinement of $[Hgua]_2 \cdot (Ti_5O_5F_{12})$: observed (line), calculated (dots), and difference (bottom) profiles of XRD data. Vertical bars are related to the calculated Bragg reflection positions.

ethanol. The mixture was heated in a Teflon autoclave under hydrothermal conditions[10] at 190 °C for 1 h using a microwave oven (CEM MARS 5). A microcrystalline powder was obtained for the Ti/*gua*/ethanol molar ratio 5:1:172. The solid product was washed with ethanol and acetone and dried at room temperature.

Characterization. Elemental analysis was performed at SCA CNRS (Solaize). Chemical analysis of $[Hgua]_2 \cdot (Ti_5O_5F_{12})$ gave the following results (atom %): Ti, 35.5; H, 1.8 (expected values: Ti, 35.86; H, 1.81). The F/Ti molar ratio, measured by energy-dispersive X-ray analysis on a Link EDX spectrometer coupled with a Hitachi S2300 scanning electron microscope, led to an experimental value of 2.3 in good agreement with the chemical formulation $[Hgua]_2 \cdot (Ti_5O_5F_{12})$ (theoretical value: 12/5 = 2.4). These analyses show that the substitution of OH/F is not significant or is very low if it exists.

Powder X-ray diffraction (XRD) patterns were collected on a MPD-PRO diffractometer (PANalytical) at room temperature between 5 and 85 °C in 2θ using Cu Kα radiation (λ = 1.5406 Å).

Structure Solution and Refinement. A C-centered orthorhombic cell was obtained from the McMaille indexing software [M(20) = 13; F(20) = 24].[11] This cell was confirmed by a satisfying whole powder pattern fit by the Le Bail method[12] using the *Fullprof* software.[13] The extracted intensities were used for the structure solution by direct space methods (*ESPOIR* software[14]) with the *Cmmm*, *Cmm*2, or *C*222 space groups. In each case, the adopted strategy consisted of the introduction of one TiF_6 octahedron, one titanium atom, and one guanidine molecule (hydrogen atoms were omitted). Similar solutions were obtained for all space groups with a reliability $R < 30\%$.

Then, Rietveld refinements were performed. A good fit was obtained with the *Cmm*2 space group (Figure 1), and the choice of a noncentrosymmetric space group was later confirmed by a positive second-harmonic-generation test. It must be noted that no distance restraint was applied. Bond-valence calculations[15] confirmed the positions of the oxygen atoms. The details of the structure determination are given in Table 1 and the X-ray atomic coordinates in Table 2. At this stage of the refinement, hydrogen atoms were omitted. The main bond lengths are indicated in Table 3.

Table 1. Crystallographic Data of $[Hgua]_2 \cdot (Ti_5O_5F_{12})$ and Refinement Parameters Obtained from Powder XRD

formula	$Ti_5F_{12}O_5N_6C_2H_{12}$
fw	667.54
cryst syst	orthorhombic
space group	*Cmm*2
a (Å)	22.410(1)
b (Å)	10.191(1)
c (Å)	3.802(1)
V (Å^3), Z	868.2(2), 2
$\rho_{calc.}$ (g·cm^{-3})	2.55
wavelength (Å)	1.54056
2θ range (deg)	5−85
no. of indep reflns	456
no. of intensity-dependent param	50
R_P, R_{wp}	0.150, 0.169
R_B, R_F	0.058, 0.056

Optical Measurements. The UV−vis diffuse-reflectance spectrum of $[Hgua]_2 \cdot (Ti_5O_5F_{12})$ was measured at room temperature between 200 and 800 nm (6.2−1.55 eV) with a 2 nm step using a Cary 5G spectrometer (Varian). This instrument was equipped with a 60-mm-diameter integrating sphere and computer-controlled with the *Scan* software. The 100% reflectance reference was obtained with Halon powder. The powder sample was sieved at 125 μm to give a homogeneous size distribution of the particles and was pressed in an adapted support to the integration sphere. The samples were irradiated under a UV lamp (λ_{exc} = 254 nm, P = 12 W, Fisher Bioblock Labosi) for various durations. The reflectivity spectra were transformed to absorption (α/S) spectra by the Kubelka−Munk function: $F(R) = \alpha/S = (1 - R)^2/2R$, where R is the reflectivity at a given wavelength, α the absorption coefficient, and S the scattering coefficient. The optical gap value was determined from the intersection of the energy axis and the extrapolated line of the linear portion at the absorption threshold.

dx.doi.org/10.1021/ic200407h |*Inorg. Chem.* 2011, 50, 5671–5678

Magnetic Measurements. The magnetic measurements were realized on one irradiated sample (48 h) with a Quantum Design MPMS-R5 SQUID magnetometer within the temperature range 2−300 K at 10 000 Oe. The sample susceptibility was corrected for the sample-holder contribution. The experimental data were adjusted with a Curie−Weiss fit: $\chi_{mol} = C/(T - \theta) + cte$, where χ_{mol} is the susceptibility per mole of titanium [emu·(Ti mol)$^{-1}$], C the Curie constant [emu·K·(Ti mol)$^{-1}$], T the temperature (K), θ the Curie−Weiss temperature (K), and cte the sum of the diamagnetic and orbital van Vleck contributions [emu·(Ti mol)$^{-1}$].

DFT Calculations. DFT calculations have been carried out using two different codes: the Vienna Ab Initio Simulation Program (VASP)[16] for geometry optimization of the structure and the *WIEN2k*[17] program package for calculation of the electronic structures and simulation of the optical properties.

The parameters used in the VASP calculations are the following. The wave functions are expanded in a plane-wave basis set with kinetic energy below 500 eV. The VASP package is used with the projected augmented wave method of Blöchl.[18] The integration of the Brillouin zone is done using the Methfessel−Paxton method on a set of k points determined by the Monkhorst−Pack scheme. All optimizations of the atomic positions follow a conjugated gradient minimization of the total energy scheme with forces smaller than 3×10^{-2} eV·Å^{-1}. The lattice parameters were fixed to be identical with the X-ray parameters.

The density of states (DOS) and optical properties are deduced from a self-consistent calculation, using the full-potential linearized augmented plane-wave method, as embodied in the *WIEN2k* code. The maximum l value in the expansion of the basis set inside the atomic sphere was 12. The convergence of the basis set was controlled by a cutoff parameter RMT × K_{max} = 4, where RMT is the smallest atomic sphere radius in the unit cell and K_{max} is the magnitude of the largest k vector. The self-consistency was carried out on a 6 k-point mesh in the irreducible Brillouin zone with the following radii: RMT(Ti) = 1.7 au, RMT(F) = 1.6 au, RMT(O) = 1.4 au, RMT(C) = 1.25 au, RMT(N) = 1.24 au, and RMT(H) = 0.67 au and with GMAX = 20 bohr^{-1}.

Table 2. Atomic Coordinates of $[Hgua]_2\cdot(Ti_5O_5F_{12})$ Refined from XRD Data

atom	site	x	y	z	B_{eq}
Ti1	8f	0.915(1)	0.816(1)	0.620(1)	3.2(1)
Ti2	2b	$^1/_2$	0	0.601(1)	3.1(1)
F1	8f	0.835(1)	0.773(1)	0.563(1)	3.2(1)
F2	8f	0.938(1)	0.634(1)	0.624(1)	4.1(1)
F3	4d	0.896(1)	1	0.603(1)	6.1(1)
F4	4e	1.000(1)	0.859(1)	0.665(1)	2.6(1)
O1	8f	0.916(1)	0.818(1)	0.105(1)	1.9(1)
O2	2b	$^1/_2$	0	0.154(1)	2.1(1)
N1	4d	0.661(1)	0	0.130(1)	4.5(1)
N2	8f	0.745(1)	0.100(1)	0.253(1)	3.6(1)
C	4d	0.717(1)	0	0.172(1)	3.7(1)

RESULTS AND DISCUSSION

Description of the Structure. The asymmetric unit of $[Hgua]_2\cdot(Ti_5O_5F_{12})$ contains two inequivalent Ti^{4+} sites, denoted as Ti1 and Ti2, which are respectively represented in blue and yellow (Figure 2). Both Ti1 and Ti2 are surrounded by four F^- and two O^{2-} ligands, forming $[TiO_2F_4]^{4-}$ octahedra. Among the four fluorine ions (Figure 2a), F3 and F4 are 2-fold-coordinated with two Ti1, while F2 is surrounded by one Ti1 and one Ti2. In contrast, F1 is only linked to Ti1. Both oxygen ions O1 and O2 are 2-fold-coordinated to two Ti1 or two Ti2, respectively (Figure 2b).

It should be noticed that the $[TiO_2F_4]^{4-}$ octahedra are significantly distorted, as was expected from the heteronature of the ligands (oxygen and fluorine). Surprisingly, only Ti2 exhibits a short Ti−O distance (d_{Ti1-O1} = 1.70 Å) characteristic of a titanyl bond. The structure of $[Hgua]_2\cdot(Ti_5O_5F_{12})$ is built up from successive $(Ti_5O_5F_{12})$ (100) layers, shifted by the C lattice translation. It is isostructural with the structure of $[Hgua]_2\cdot(Al_5F_{17})$ recently published by Adil et al.[19] These (100) layers, resulting from the intergrowth of HTB and perovskite columns, are separated by guanidinium cations in which the N2 atoms are close to nonbonding F1 atoms (Figure 2a). The $(Ti_5O_5F_{12})^{2-}$ layers can also be described from the association with the fluorine corners (F2, F3, and F4) of two types of infinite chains $_\infty(TiOF_4)$ based on O1-corner-sharing Ti1-based octahedra and O2-corner-sharing Ti2-based octahedra (Figure 2b).

The Rietveld crystal structure has been used as the starting point of the DFT geometry optimization calculations. Hydrogen atoms were geometrically introduced to describe properly the interactions between the inorganic $(Ti_5O_5F_{12})^{2-}$ layers and the organic $[Hgua]^+$ cations. Three inequivalent hydrogen positions (H1, H2, and H3) were generated using the *CRYSTAL* software.[20] All atoms were then allowed to relax during the DFT geometry optimization. The resulting atomic coordinates are listed in Table S1

Table 3. Selected Interatomic Distances (Å) of the X-ray Structure and Geometry-Optimized Model of $[Hgua]_2\cdot(Ti_5O_5F_{12})$

	X-ray model distance [Å]	DFT model distance [Å]	Variation (%) $(d_{DFT} - d_{X\text{-}ray})/d_{X\text{-}ray}$
Ti1−F1	1.856(1)	1.876	1.1
Ti1−F2	1.930(1)	1.989	3.1
Ti1−F3	1.921(1)	1.941	1.0
Ti1−F4	1.957(1)	1.991	1.7
Ti1−O1	1.843(1)	1.711	−7.2
Ti1−O1	1.958(1)	2.096	7.0
Ti2−F2 (×4)	1.952(1)	1.945	−0.4
Ti2−O2	1.699(1)	1.697	−0.1
Ti2−O2	2.103(1)	2.104	0.0
C−N1	1.261(1)	1.329	5.4
C−N2 (×2)	1.243(1)	1.333	7.2
N1−H3		1.013	
N2−H1		1.016	
N2−H2		1.019	

dx.doi.org/10.1021/ic200407h |*Inorg. Chem.* 2011, 50, 5671–5678

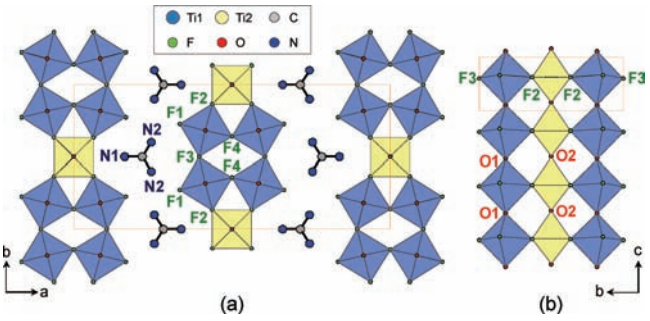

Figure 2. XRD-refined crystal structure of $[Hgua]_2 \cdot (Ti_5O_5F_{12})$ viewed along (a) the *c* axis and (b) the *a* axis.

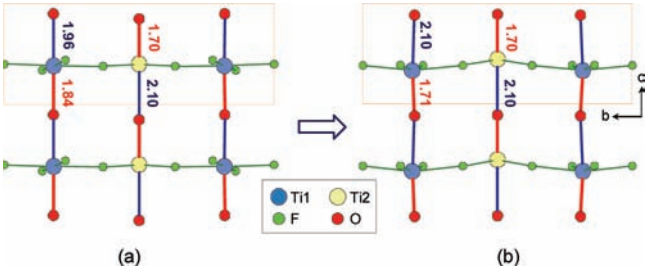

Figure 3. Schematic view of the local atomic arrangement around the nonequivalent titanium Ti1 and Ti2 sites (a) before and (b) after the DFT geometry optimization. Short (titanyl) and long Ti−O bonds are represented in red and blue, respectively.

of the Supporting Information. The main optimized bond lengths are indicated in Table 3.

Figure 3 shows the local arrangement around the Ti1 and Ti2 atoms before (a) and after (b) the DFT geometry optimization. Interestingly, both Ti1 and Ti2 exhibit one short titanyl bond (d_{Ti1-O1} = 1.71 Å and d_{Ti2-O2} = 1.70 Å) and one longer Ti−O bond (d_{Ti1-O1} = 2.10 Å and d_{Ti2-O2} = 2.10 Å) in the optimized model. Consequently, the distortion is similar for Ti1 and Ti2, in contrast to the Rietveld refinement. In a previous paper,[21] a similar observation for an hybrid system containing vanadyl bonds was encountered. It should be noticed that the optimized structure leads to an alternation of short and long Ti−O bonds in the infinite chains $_\infty(TiOF_4)$ oriented along the *c* axis (Figure 3b). Such a cooperative distortion is also present in other d^0 transition metal (Ti^{4+}, Nb^{5+}, and W^{6+}) compounds and can be explained based on the second-order Jahn−Teller theorem.[22−24]

The interactions between the inorganic and organic parts in $[Hgua]_2 \cdot (Ti_5O_5F_{12})$ are also affected by the DFT geometry optimization. As illustrated in Figure 4, two main atomic rearrangements of the $[Hgua]^+$ cations occur: (1) an elongation of the C−N distances and (2) a rotation of the NH_2 group related to the N2 sites. The average C−N bond length increases from 1.25 to 1.33 Å in the X-ray and DFT models, respectively; the last distance is in perfect agreement with the previously reported distances.[19,25] In addition, the geometry of the $[Hgua]^+$ cations is better described with N−C−N bond angles close to 120° in the DFT model (119.75, 120.08, and 120.08°) compared to the Rietveld model (110.35, 122.80, and 122.80°). Finally, the N2−N1−N2−C dihedral angle decreases from 14° in the Rietveld model to 2° in the DFT model. Then the DFT model better describes the planar sp^2 geometry of such a strongly delocalized π system. The rotation of $N2H_2$ groups implies the shortening of

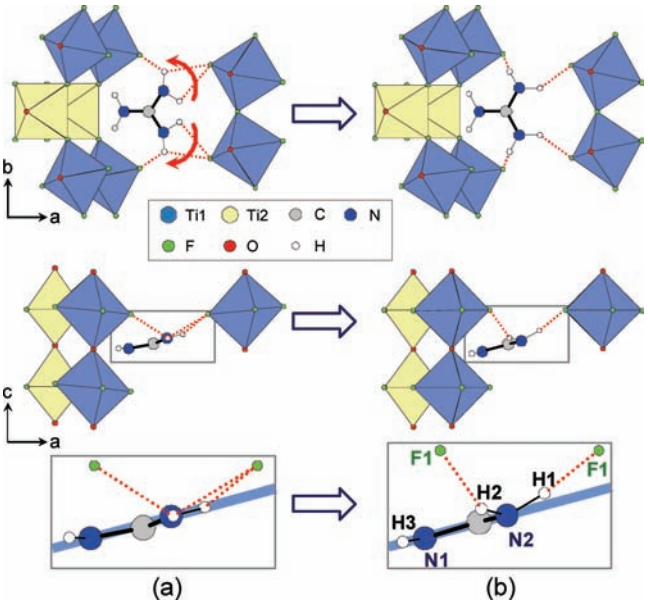

Figure 4. Schematic view of the local atomic arrangement around an $[Hgua]^+$ cation (a) before and (b) after the DFT geometry optimization. Hydrogen bonds are represented by red dotted lines.

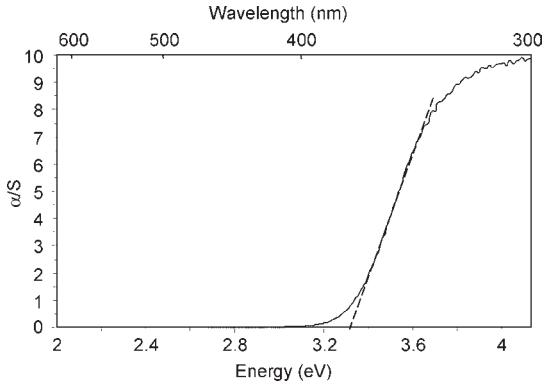

Figure 5. UV−vis diffuse-reflectance spectrum of $[Hgua]_2 \cdot (Ti_5O_5F_{12})$, after application of the Kubelka−Munk transformation.

the H···F distances in N2−H1···F1 and N2−H2···F1 from 2.389 to 2.319 Å and from 1.961 to 1.881 Å, respectively, and the opening of N−H···F bond angles from 96.4 to 144.8° and from 101.2 to 140.9°. It is clear that hydrogen bonds are strengthened; when taken into account, they could compensate for the abnormally small bond-valence sum (0.77 and 0.73 in X-ray and DFT models, respectively) for the F1 atom (see Tables S2 and S3 of the Supporting Information).[26]

Optical Properties. The UV−vis diffuse-reflectance spectrum of $[Hgua]_2 \cdot (Ti_5O_5F_{12})$, after application of the Kubelka−Munk transformation, is displayed in Figure 5. A well-defined absorption threshold can be extracted at about 3.32 eV. This value is similar to that of the oxyfluorotitanate $TiOF_2$.[6] As in $TiOF_2$, the origin of this optical gap in $[Hgua]_2 \cdot (Ti_5O_5F_{12})$ is supposed to be related to the O(2p) → Ti(3d) transition. However, to ensure such a hypothesis, the nature of the chemical bonds in $[Hgua]_2 \cdot (Ti_5O_5F_{12})$ was first analyzed by calculating the total (tDOS) and a set of partial (pDOS) density of states (Figure 6).

dx.doi.org/10.1021/ic200407h |*Inorg. Chem.* 2011, 50, 5671–5678

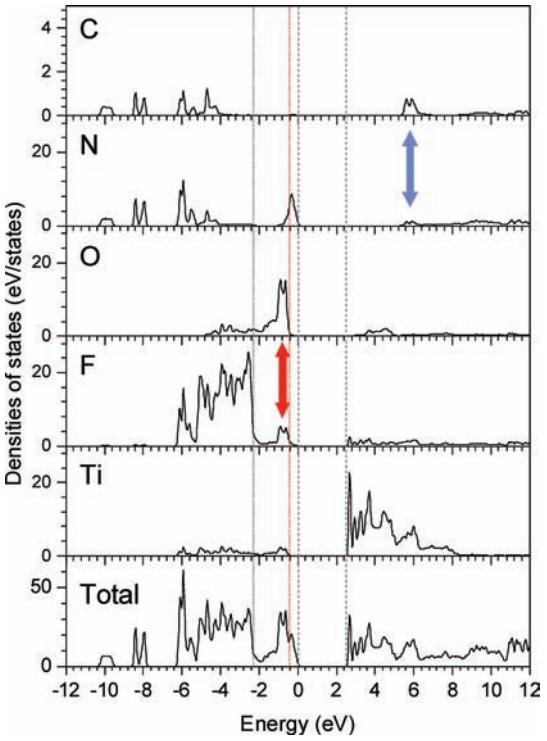

Figure 6. tDOS and pDOS (C, N, O, F, and Ti) of the optimized structure of $[Hgua]_2 \cdot (Ti_5O_5F_{12})$. The Fermi level is set to 0 eV; the top of the valence band and the bottom of the conduction band are denoted with gray dashed lines. The red and green dotted lines indicate the top of the O(2p) and F(2p) bands, respectively.

DOS Calculations. First of all, the fundamental band gap, deduced from DFT calculations, is 2.4 eV. Below the Fermi level, the occupied band, i.e., the valence band (VB), is based on three main blocks, which partly overlap in energy: a N(2p) block from 0 to −10 eV, an O(2p) block from −0.3 to −4.7 eV, and a F(2p) block from −0.3 to −6.3 eV.

The N(2p) block could be decomposed into two main areas: the first part, from 0 to −0.8 eV, and the second part, from −3.8 to −10 eV, which interact slightly and strongly, respectively, with the C(2p) states, as illustrated by the relative intensities of the nitrogen and carbon pDOS (Figure 6). These interactions are the direct signature of the covalent C−N chemical bond constituting the skeleton of the organic part.

On the other side, a close inspection of the O(2p) and F(2p) blocks evidences that, in addition to being in the same energy region, they exhibit similar shapes, confirming that these orbitals are interacting (see the red double arrow in Figure 6). The O(2p)−F(2p) interaction is indirect and is mediated by the Ti(3d) states, as confirmed by inspection of the titanium pDOS. In other words, in the inorganic part, the Ti^{4+} cation, by interacting simultaneously with O^{2-} and F^- anions, induces a mixed character in both the O(2p) and F(2p) bands, which will affect the optical properties of this compound, as we will discuss below.

Above the Fermi level, the first empty states, i.e., conduction band (CB), are mainly based on Ti(3d) orbitals interacting with F(2p) and O(2p) orbitals (2.4−8.5 eV). It should be noticed that the C(2p) states appear also in the energy region 5.4−6.3 eV and interact with the N(2p) states of the organic part of the compound.

The present analysis of pDOS confirms that organic−inorganic interactions in $[Hgua]_2 \cdot (Ti_5O_5F_{12})$ are weak and are limited to hydrogen bonds. Thus, to simplify the interpretation of the optical properties of $[Hgua]_2 \cdot (Ti_5O_5F_{12})$ in terms of optical transitions, it appears relevant to gather the states of $[Hgua]^+$ and $(Ti_5O_5F_{12})^{2-}$ in two different figures. The main DOS features around the Fermi level are summed up in a schematic way in Figure 7, and the related optical transitions are highlighted in Figure 8. These optical transitions have been estimated based on calculation of the dielectric function $\varepsilon(\omega) = \varepsilon_1(\omega) + i\varepsilon_2(\omega)$,

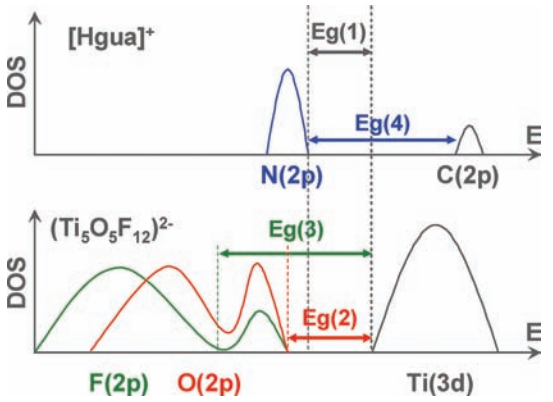

Figure 7. DOS schemes of a set of atomic orbitals involved in the organic and inorganic parts of $[Hgua]_2 \cdot (Ti_5O_5F_{12})$. Four band gaps are defined and correspond to the fundamental Eg(1), inorganic Eg(2) [O(2p)−Ti(3d)] and Eg(3) [F(2p)−Ti(3d)], and organic Eg(4) band gaps.

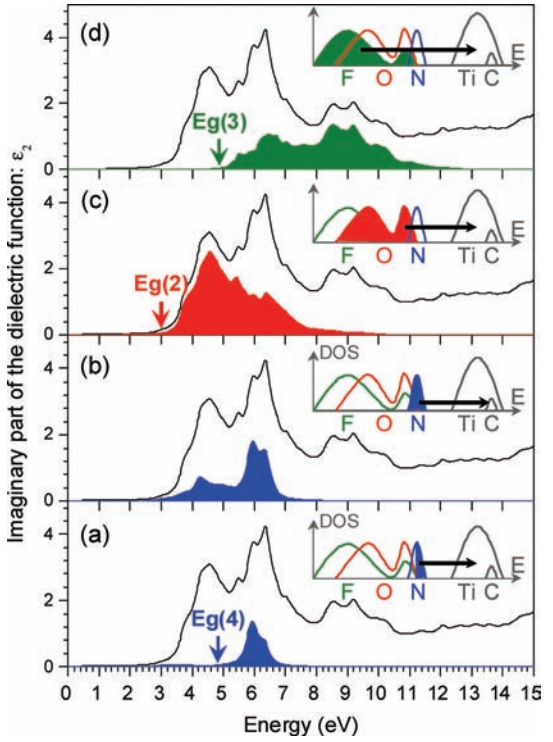

Figure 8. DFT prediction of the imaginary part of the dielectric function as a function of the incident photon energy (solid line). The optical transitions coming from the N(2p), O(2p), and F(2p) majority bands are represented in blue, red, and green, respectively. In each case, the nature of the optical transition is schematically represented with a DOS (the filled part indicates the initial states for the transition).

which gives access to the diffusion (ε_1) and absorption (ε_2) properties of $[Hgua]_2\cdot(Ti_5O_5F_{12})$. More specifically, the total absorption power of $[Hgua]_2\cdot(Ti_5O_5F_{12})$ is given in Figure 8 (solid line) and the O(2p) → Ti(3d), F(2p) → Ti(3d), and N(2p) → C(2p) transitions are highlighted by red-, green-, and blue-filled areas, respectively.

Analysis of the organic- and inorganic-related DOS allows one to better understand the nature of the band gaps in such hybrid systems, leading to the definition of four main band gaps, Eg(1) ≈ 2.4 eV, Eg(2) ≈ 3.0 eV, Eg(3) ≈ 4.8 eV, and Eg(4) ≈ 5.4 eV, for the fundamental band gap (from total DOS) and O(2p) → Ti(3d), F(2p) → Ti(3d), and N(2p) → C(2p) optical transitions. From Figure 7, it is clear that Eg(1) is defined from the top of the organic VB to the bottom of the inorganic CB. However, these states are not chemically connected [spatial separation between the N(2p) and Ti(3d) orbitals], and no optical transition starting at this energy value is expected.

It should be noticed that estimation of the N(2p) → C(2p) transition has been done after careful analysis of the character of the initial bands, which contain O(2p), F(2p), and N(2p) states in the same energy range, even if not interacting (Figure 8a). The resulting partial optical absorption, associated with the N(2p) → C(2p) transition, starts at Eg(4) ≈ 5.4 eV. Although the fundamental band gap is significantly smaller [Eg(1) ≈ 2.4 eV], the N(2p) states do not interact with the Ti(3d) states, as expected, but only with the C(2p) states. Such a feature is of interest because the first states at the top of the VB are not involved in the optical absorption processes in the visible range (1.5−3.1 eV).

Thus, the first absorption peak arises from the O(2p) → Ti(3d) transition and the DFT optical gap estimated from the tangent method is about 3.2 eV, i.e., in very good agreement with the experimental value deduced from diffuse-reflectance measurements. It should be noticed that the present agreement is not expected because DFT usually underestimates the band gaps. Indeed, the optical absorptions start at about Eg(2) with a steep threshold, which is directly related to the nature of the O1 pDOS near the Fermi level (see Figure S1 of the Supporting Information). The broad appearance of the resulting absorption band ranging from 3 to more than 8 eV is the signature of the mixed nature of the initial O(2p) states interacting with F(2p) and residual noninteracting N(2p) states (Figure 6).

The present analysis of the optical properties shows that the absorption originates first from the O(2p) → Ti(3d) transition and is further enhanced by the F(2p) → Ti(3d) transition. A similar behavior is encountered in $TiOF_2$.[6] However, the N(2p) → C(2p) transition adds a significant contribution centered at ≈6 eV (Figure 8a). Then, both the organic and inorganic parts contribute nearly separately to the optical absorption of $[Hgua]_2\cdot(Ti_5O_5F_{12})$.

Figure 9 gives the evolution of the refractive index (n) as a function of the energy $\hbar\omega$ for $[Hgua]_2\cdot(Ti_5O_5F_{12})$ and the TiO_2 rutile. Similarly to the dielectric function, the refractive index is a complex function: $N(\omega) = n(\omega) + ik(\omega)$ (k = extinction coefficient). In the low-energy region, it is clear that the refractive index of $[Hgua]_2\cdot(Ti_5O_5F_{12})$ is significantly smaller than that of the TiO_2 rutile. For instance, at 2.1 eV, $n([Hgua]_2\cdot(Ti_5O_5F_{12}))$ = 1.94 and $n(TiO_2)$ = 2.88. The refractive index difference between $[Hgua]_2\cdot(Ti_5O_5F_{12})$ and an organic medium (n ≈ 1.5 eV) is then small and, consequently, the whitening effect, which affects TiO_2 embedded in such an organic medium, will be significantly reduced.

Photochromic Properties. The photoreduction of Ti^{4+} to Ti^{3+} under UV-light irradiation has been reported by Brohan et al. for titanium dioxide gels, which are nanostructured hybrid organic−inorganic materials.[29] Such materials are investigated for their potential interest as electron−hole pair generators for solar to electrical power conversion applications.

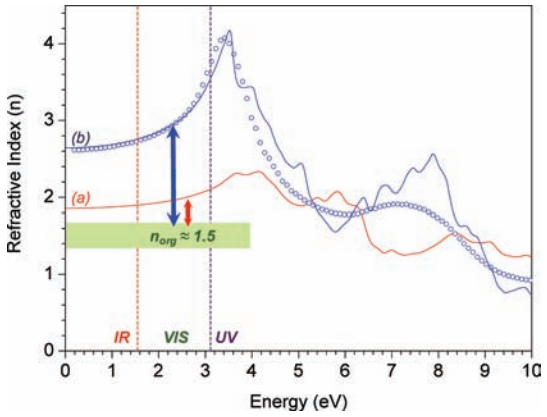

Figure 9. Refractive indices of (a) $[Hgua]_2\cdot(Ti_5O_5F_{12})$ and (b) TiO_2 determined from EELS experiments (open circles) and DFT calculations (solid lines). The blue and red double arrows define the difference between the refractive indices of an embedded organic medium ($n_{org} \approx 1.5$; see the green rectangular region) and TiO_2 and $[Hgua]_2\cdot(Ti_5O_5F_{12})$, respectively.

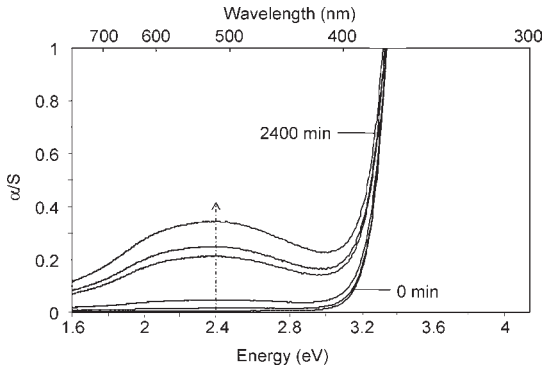

Figure 10. Evolution of the reflectance after the Kubelka−Munk transformation of $[Hgua]_2\cdot(Ti_5O_5F_{12})$ versus the energy after irradiation at 254 nm for various durations (0, 10, 60, 1020, 1440, and 2400 min).

Similarly, this question can be addressed for the present hybrid compound by evaluating its ability to generate electron−hole pairs under UV irradiation. Such a property could be probed by looking at the evolution under UV irradiation of two different properties: (i) the optical properties (color) and (ii) the magnetic properties (paramagnetic centers).

Figure 10 shows the evolution of the optical properties of $[Hgua]_2\cdot(Ti_5O_5F_{12})$ with the time of exposure to UV excitation at λ = 254 nm (i.e., E = 4.9 eV). A broad absorption band centered at around λ = 517 nm (i.e., E = 2.4 eV) appears, and its intensity increases with the irradiation duration. Such a photochromic response of $[Hgua]_2\cdot(Ti_5O_5F_{12})$ is also identified by the slight color change of the sample (negligible for an excitation at λ = 365 nm): the color of the powder evolves from white to light purple-gray, and the color density increases with the time of UV exposure. The color saturation is observed after 2400 min. The origin of this photochromic effect is well-known in hybrid materials such as polyoxometalates[27,28] and has also been evidenced in titanium oxide gels.[29]

dx.doi.org/10.1021/ic200407h |Inorg. Chem. 2011, 50, 5671–5678

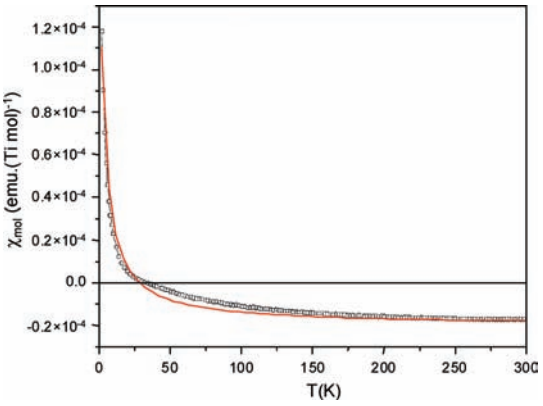

Figure 11. Temperature dependence of the magnetic susceptibility (open circles) of $[Hgua]_2 \cdot (Ti_5O_5F_{12})$ after irradiation for 40 h. The red line corresponds to the fitting curve.

In the present case, UV excitation induces the promotion of electrons from the O(2p) VB to the Ti(3d) CB, leading to the creation of electron−hole pairs. The photogenerated electron is then trapped on a Ti(3d) state, leading to modification of the titanium oxidation degree: $Ti^{IV}(3d^0) + e^- \rightarrow Ti^{III}(3d^1)$. The so-obtained Ti^{3+} photoreduced center could absorb visible light through d−d transitions and intervalence charge-transfer processes, which induce the observed coloration.

To confirm the eventual presence of Ti^{III} photoreduced centers in $[Hgua]_2 \cdot (Ti_5O_5F_{12})$ after UV irradiation at λ = 254 nm, magnetic measurements have been realized after 48 h of UV irradiation (Figure 11). The fit of the experimental susceptibility with a Curie−Weiss model gives C = 0.000 63 emu·K·(Ti mol)$^{-1}$, θ = −2.8 K, and cte = -2×10^{-5} emu·(Ti mol)$^{-1}$. The negative value of the Curie−Weiss temperature θ is indicative of weak antiferromagnetic interactions between Ti^{III} cations. A similar result was found for the TiO_2 gels of Brohan et al.[29] with a Curie constant C = 0.3492 emu·K·(Ti mol)$^{-1}$. In $[Hgua]_2 \cdot (Ti_5O_5F_{12})$, the proportion of Ti^{III} sites is approximately 0.2%. This small value is probably due to a reduction of the superficial value of the UV-irradiated crystallite and the absence of bulk contribution.

CONCLUSION

A new generation of hybrid organic−inorganic Ti-based UV absorbers with low refractive indices have been prepared by microwave-heating-assisted hydrothermal synthesis: $[Hgua]_2 \cdot (Ti_5O_5F_{12})$. The crystal structure has been accurately determined from powder XRD data by combining a direct space method, Rietveld refinement, and DFT geometry optimization. $[Hgua]_2 \cdot (Ti_5O_5F_{12})$ crystallizes in the orthorhombic crystal system, *Cmm*2 space group, and the following lattice parameters: a = 22.410 (1) Å, b = 11.191 (1) Å, and c = 3.802 (1) Å.

The simulated optical response related to the DFT-optimized atomic structure leads to a theoretical optical gap value of about 3.2 eV, in very good agreement with the experimental value of 3.3 eV, estimated using UV−vis diffuse reflectivity. Analysis of the DFT data shows that the band gap is mainly related to the O(2p) → Ti(3d) transition. More specifically, it is shown that the fundamental band gap of 2.4 eV from N(2p) VB to Ti(3d) CB is not optically active because of the spatial separation of these two elements. Such a feature is of interest because the first states at the top of the VB are not involved in the optical absorption processes encountered in the visible range (1.5−3.1 eV). Thus, the creation of holes in these VB states by cationic doping with Al^{3+} would allow one to tune the electronic properties without changing the optical properties of the material. Such a feature could be of direct interest for the preparation of new p-type transparent conducting oxide materials. It is interesting to note that $[Hgua]_2 \cdot (Al_5F_{17})$ is isostructural with $[Hgua]_2 \cdot (Ti_5O_5F_{12})$.

In terms of UV-shielding application, $[Hgua]_2 \cdot (Ti_5O_5F_{12})$ exhibits an adequate band gap and a low refractive index ($n \approx$ 1.9) with respect to TiO_2 ($n \approx$ 2.7). As a consequence, such particles embedded in an organic medium for UV protection will lead to a significantly enhanced transparency in the visible range. The presence of a low-scattering element (fluorine) and of organic spacers between the inorganic blocks is responsible for a strong refractive index reduction.

Finally, the ability to produce photogenerated electron−hole pairs in $[Hgua]_2 \cdot (Ti_5O_5F_{12})$ under UV excitation has been considered. The optical and magnetic measurements evidence a small amount of Ti^{3+} photoreduced centers after UV irradiation, characterized by a weak photochromic behavior and the presence of antiferromagnetic interactions.

In conclusion, the joined experimental and theoretical investigations of the atomic structure and optical properties of $[Hgua]_2 \cdot (Ti_5O_5F_{12})$ evidence the interest of this hybrid fluoride for UV shielding: the optical band gap is 3.3 eV, the absorption threshold is steep, and the refractive index is 1.9. Such a material could then be considered for potential applications as protective UV absorbers, in the replacement of ZnO or TiO_2. However, the long-term stability remains to be evaluated.

ASSOCIATED CONTENT

Supporting Information. Atomic coordinates, selected interatomic distances, and total and partial DOS. This material is available free of charge via the Internet at http://pubs.acs.org.

AUTHOR INFORMATION

Corresponding Author

*E-mail: martine.bujoli@cnrs-imn.fr (M.B.-D.), vincent.maisonneuve@univ-lemans.fr (V.M.).

ACKNOWLEDGMENT

The authors are indebted to Prof. C. Payen for his help in monitoring the susceptibility measurements. The computational work was carried out at the Centre Régional de Calcul Intensif des Pays de la Loire (CCIPL) and financed by the French Research Ministry, the Région Pays de la Loire, and Nantes University. Thanks are also due to the Région des Pays de la Loire for a doctoral grant (to J.L.; the Perle project).

REFERENCES

(1) Tu, Y.; Zhou, L.; Jin, Y. Z.; Gao, C.; Ye, Z. Z.; Yang, Y. F.; Wang, Q. L. *J. Mater. Chem.* **2010**, *20*, 1594.

(2) de Lima, J. F.; Martins, R. F.; Neri, C. R.; Serra, O. A. *Appl. Surf. Sci.* **2009**, *255*, 9006.

(3) Zhang, D.; Niu, F.; Li, H.; Shi, L.; Fang, J. *Powder Technol.* **2011**, *207*, 35.

(4) Goubin, F.; Rocquefelte, X.; Whangbo, M.-H.; Montardi, Y.; Brec, R.; Jobic, S. *Chem. Mater.* **2004**, *16*, 662.

(5) Masui, T.; Fujiwara, K.; Machida, K.; Adachi, G. *Chem. Mater.* **1997**, *9*, 2197.

(6) Rocquefelte, X.; Goubin, F.; Montardi, Y.; Viadere, N.; Demourgues, A.; Tressaud, A.; Whangbo, M.-H.; Jobic, S. *Inorg. Chem.* **2005**, *44*, 3589.
(7) Demourgues, A.; Penin, N.; Durand, E.; Weill, F.; Dambournet, D.; Viadere, N.; Tressaud, A. *Chem. Mater.* **2009**, *21*, 1275.
(8) Mazzocchetti, L.; Cortecchia, E.; Scandola, M. *Appl. Mater. Interfaces* **2009**, *1*, 726.
(9) Rocquefelte, X.; Goubin, F.; Koo, H.-J.; Whangbo, M.-H.; Jobic, S. *Inorg. Chem.* **2004**, *43*, 2246.
(10) Adil, K.; Goreshnik, E.; Courant, S.; Dujardin, G.; Maisonneuve, V.; Leblanc, M. *Solid State Sci.* **2004**, *6*, 1229.
(11) Le Bail, A. *Powder Diffraction* **2004**, *19*, 249.
(12) Le Bail, A.; Duroy, H.; Fourquet, J.-L. *Mater. Res. Bull.* **1988**, *23*, 447.
(13) Rodriguez-Carvajal, J. *Physica B* **1993**, *55*, 192.
(14) Le Bail, A. *Mater. Sci. Forum* **2001**, *65*, 378.
(15) Brese, N. E.; O'Keefe, M. *Acta Crystallogr.* **1991**, *B47*, 192.
(16) Kresse, G.; Furthmuller, J. *Phys. Rev. B* **1996**, *54*, 514.
(17) Blaha, P.; Schwarz, K.; Madsen, G. K.; Kvasnicka, D.; Luitz, J. *WIEN2k, An Augmented Plane Wave and Local Orbitals Program for Calculating Crystal Properties*; 2001.
(18) Blöchl, P. E. *Phys. Rev. B* **1994**, *50*, 17953.
(19) Adil, K.; Le Bail, A.; Leblanc, M.; Maisonneuve, V. *Inorg. Chem.* **2010**, *49*, 2392.
(20) Betteridge, P. W.; Carruthers, J. R.; Cooper, R. I.; Prout, K.; Watkin, D. J. *J. Appl. Crystallogr.* **2003**, *36*, 1487.
(21) Djerdj, I.; Cao, M.; Rocquefelte, X.; Cerny, R.; Jaglicic, Z.; Arcon, D.; Potocnik, A.; Gozzo, F.; Niederberger, M. *Chem. Mater.* **2009**, *21*, 3356.
(22) Kunz, M.; Brown, I. D. *J. Solid State Chem.* **1995**, *115*, 395.
(23) Wheeler, R. A.; Whangbo, M.-H.; Hughbanks, T.; Hoffmann, R.; Burdett, J. K.; Albright, T. A. *J. Am. Chem. Soc.* **1986**, *108*, 2222.
(24) Ra, H.-S.; Ok, K. M.; Halasyamani, P. S. *J. Am .Chem. Soc.* **2003**, *125*, 7764.
(25) Bharatam, P. V.; Iqbal, P.; Malbe, A.; Tiwari, R. *J. Phys. Chem. A* **2004**, *108*, 10509.
(26) Le Bail, A.; Mercier, A.-M. *Acta Crystallogr.* **2009**, *E65*, i23.
(27) Yamase, T. *Chem. Rev.* **1998**, *98*, 307.
(28) Coué, V.; Dessapt, R.; Bujoli-Doeuff, M.; Evain, M.; Jobic, S. *Inorg. Chem.* **2007**, *46*, 2824.
(29) Cottineau, T.; Brohan, L.; Pregelj, M.; Cevc, P.; Richard-Plouet, M.; Arcon, D. *Adv. Funct. Mater.* **2008**, *18*, 2602.